# Granular avalanches in a two-dimensional rotating drum with imposed vertical vibration

Daniel L. Amon, Tatiana Niculescu, and Brian C. Utter*
*Department of Physics and Astronomy, James Madison University, Harrisonburg, Virginia 22807, USA*
(Received 24 September 2012; revised manuscript received 22 March 2013; published 11 July 2013)

We present statistics on granular avalanches in a rotating drum with and without imposed vertical vibration. The experiment consists of a quasi-two-dimensional, vertical drum containing pentagonal particles and rotated at a constant angular velocity. The drum rests on an electromagnetic shaker to allow vibration of the assembly as it rotates. We measure time series of the slope of the interface and find that the critical angle for slope failure $\theta_c$ and the resulting angle of repose $\theta_r$ are broadly distributed with an approximate power-law distribution of avalanches $\theta_c - \theta_r$ for large avalanches. The faceted pentagonal grains used lead to significant interlocking with critical and repose angles ($\theta_c \approx 45^\circ$ and $\theta_r \approx 39^\circ$) larger than experiments using spherical grains, even with vibration, and avalanche magnitudes correlated with the prior build-up and anti-correlated with the prior avalanche. We find that the stability of the assembly increases with small vibrations and is destabilized at vibration amplitudes above a dimensionless acceleration (peak acceleration divided by acceleration due to gravity) of $\Gamma = 0.2$. We also study history dependence of the avalanches by periodically oscillating the drum to compare the initial avalanche upon reversal of shear to steady-state distributions for avalanches during continuous rotation. We observe history dependence as an initial decrease in critical angle upon reversal of the drum rotation direction, indicating that a texture is induced to resist continued shear such that the surface is weaker to reversals in shear direction. Memory of this history is removed by sufficient external vibration ($\Gamma \geqslant 0.8$), which leads to compaction and relaxation of the surface layer grains responsible for avalanching dynamics, as initial and steady-state avalanche distributions become indistinguishable.

DOI: 10.1103/PhysRevE.88.012203 PACS number(s): 45.70.Ht, 81.05.Rm, 83.80.Fg

## I. INTRODUCTION

Avalanches in granular systems are examples of the unpredictable nature of complex materials. Free surface flows are one category of dense flows currently receiving considerable attention [1,2] and appear in a variety of contexts, from natural avalanches [3] to mixing in industrial hoppers [4]. Typically a granular slope fails if it is above a critical angle, and it reaches a characteristic angle of repose after failure. However, individual events are unpredictable and intermittent, and there is a range of observed angles for both failure and repose.

In the case of a static granular slope, grains are prevented from reaching the lowest energy state (i.e., a flat surface) due to frictional contacts and geometric constraints. In a generic model of a jammed system [5], geometrically frustrated grains can be freed to initiate motion by either increased shear, decreased density, or added vibrational energy (i.e., "granular temperature"). While density is self-selected in a gravity-driven flow, global shear can be increased by tilting the pile. Imposed vibrational energy can then serve as an additional control parameter that can be tuned independently to affect stability, flow, and mixing of granular samples.

Recent studies on stability have focused on failures of a granular slope [6], precursor events leading to failure [7], and avalanche dynamics in the rotating drum geometry specifically [7–9]. The rotating drum geometry allows continuous driving of a granular or multiphase system to allow well-controlled and arbitrarily long experimental measurements of properties such as the flow profile and particle trajectories [10–13]. With long data runs, statistics reveal nontrivial correlations between failure and repose angles [8] and intermittency between avalanching and continuous flow behavior [9]. Some of the characteristic features of granular flow in a rotating drum flow include rigid body rotation of the bulk with particle motion confined to the surface layer [10–12] and both particle mixing and segregation occurring in this surface layer flow [4,13,14].

Vibration has long been used to input energy to continuously drive granular systems, leading to effects such as compaction and dilation [15,16], surface instabilities [17,18], and reduced resistance to intruder particles driven through the granular material [19]. Studies of jamming and unjamming phenomena in particular and vibration-induced flows have been performed with vertical or horizontal vibration [20–25] or the simultaneous application of both [26]. There has also been interest recently in characterizing related phenomena, such as the precursors before avalanches and the degree to which frictional contacts are mobilized [27,28]. Attempts to develop a theoretical model for the angle of repose under external vibration have focused on mean-field approaches, such as a mesoscopic theory of granular avalanches under vertical vibration [29] and a model based on fluctuations in local density or dilatancy to account for the metastability observed in the angle of repose [30], but a predictive theory is still lacking.

While increasing vibration typically leads to failure, we find that small vibrations lead to strengthening of the pile. Similar results were observed by Rubin *et al.*in which horizontally shaking the grains before tilting the pile resulted in larger shaking accelerations needed to induce failure of the surface [25]. It is known that agitation or tapping can lead to compaction and local ordering [15,31], which would lead to strengthening of the pile due to the sensitive dependence of shear modulus on packing fraction. Pentagonal grains used here in a confined system also result in strong interlocking [32] and much steeper critical angles than observed in experiments using spherical grains [33]. For instance, even for accelerations

*utterbc@jmu.edu

 

well above the acceleration due to gravity, we do not find logarithmic relaxation to a flat surface as has been observed in experiments with spherical grains under vibration [20].

One characteristic of granular materials leading to their unpredictability is that they are particularly history dependent, since the preparation of the assembly determines the frictional forces at contacts. This hysteresis is frequently attributed to anisotropy in the particle-averaged contact or force network [34,35], or equivalently, as the deviatoric component of the fabric tensor and stress tensor, respectively [36]. That is, shear induces anisotropy in the contact and force networks, or texture [36], which produces anisotropy in the shear modulus, with a strong force network oriented to resist further shear.

There are a number of examples where this history-dependent texture is revealed. In shearing experiments, reversing the shear direction results in an initial weakening of a granular material, in which smaller forces and larger grain motion relative to continuous shear are observed, as force chains opposing the motion rearrange to respond to the new shear [34,37]. Similarly, oscillatory motion in simulations of a rotating drum are found to exhibit clear history dependence in volumetric strain, fabric anisotropy, and principal stress direction, particular in the weak force network [35]. Disrupting the existing texture also impacts behavior of granular systems. For instance, mechanically disturbing the surface layers of a slope created by avalanching grains was found to reduce the critical angle for failure [38], and the rheology of static granular materials was recently shown to exhibit nonmonotonic stress-strain relationships and hysteresis, with significant effects of vibration at low shear rates, including a reduction in the hysteresis [39].

In this paper we present experiments on granular materials in a rotating drum with and without imposed vertical vibrations. We study a two-dimensional photoelastic system, which allows measurement of both particle positions and stresses. We measure time series of the average angle of the surface relative to horizontal $\theta(t)$ and impose vibrations characterized by a dimensionless acceleration $\Gamma = A(2\pi f)^2/g$ [18,40], given the amplitude $A$ and frequency $f$ of the vibration and the acceleration due to gravity $g$. The pentagonal grains used presently exhibit significant geometrical frustration, with larger mean critical and repose angles and broad, overlapping distributions of critical and repose angles, unlike spherical grains [8,20,33]. We find that the probability for an avalanche to occur decreases as a power law with the magnitude of the avalanche, as measured by the change in angle of the surface $\Delta\theta$ during the avalanche, as in similar systems [41]. In addition, we find that with small vibrations ($\Gamma \lesssim 0.2$), a strengthening of the pile is observed, and larger critical angles are reached before failure, while larger imposed vibrations lead to failure of the slope and a smaller critical angle.

We find the system to be history dependent and that reversing the direction of rotation initially leads to decreased stability of the slope. This history dependence is eliminated with sufficient external vibration ($\Gamma \geqslant 0.8$) as increased agitation, compaction, and restructuring of frictional contacts leads to a loss of memory of the system's history. Measurements of the effect of vibration on a stationary, tilted interface and stresses in the photoelastic grains during avalanching show that failure is localized at the surface and that vibration leads to disturbance of these surface layers with little rearrangement throughout the bulk.

In this paper we discuss the experiment in detail. In Sec. III we present data on steady-state avalanches without external vibrations. In Sec. IV we study the effects of added external vibrations. We then focus on the history dependence of the slope by looking at an oscillating drum, with and without vibration, in Sec. V.

## II. EXPERIMENTAL METHODS

The experiment consists of a quasi-two-dimensional, rotating circular drum filled with pentagonal grains as shown in Fig. 1. The rotating drum is a commonly used experimental geometry that allows for arbitrarily long data runs to study time series of the interfacial slope versus time as discussed above.

The drum is oriented vertically and filled with a single layer of pentagonal photoelastic particles ($d \approx 7$ mm, drum diameter $= 58$ cm $\approx 85\ d$). The separation between the walls in the drum is slightly larger than the thickness of the particles (3 mm), and a dry lubricant is used to minimize friction with the wall. Use of photoelastic particles in two dimensions allows both particle tracking and imaging of the force network. Approximately 2600 grains are placed into the circular drum, such that the drum is slightly less than half full.

The drum is placed on top of a wheel driven by a stepper motor and rotates at a constant rate, approximately one revolution every 10 min (≈0.001 Hz) in the present study, such that the experiment remains in the quasistatic regime. In this regime, individual avalanches are discrete events in time, the observed behavior is independent of velocity, and statistics characterizing the flow depend only on the angular displacement of the drum. The driving wheel is attached to the motor

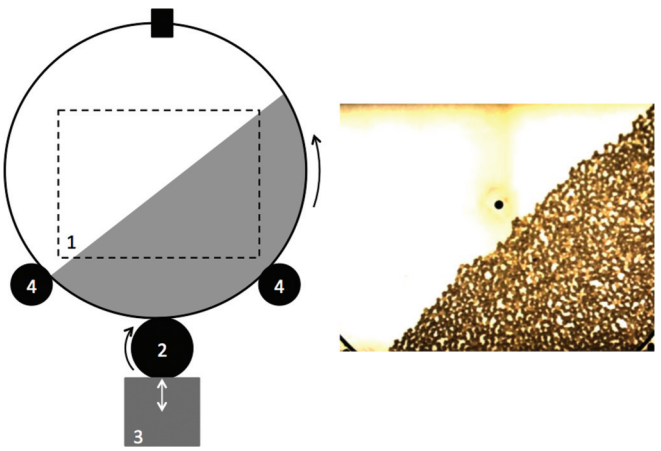


FIG. 1. (Color online) Schematic of two-dimensional (2D) rotating drum experiment (left) and typical experimental image (right). The grains are contained in a single layer between two acrylic disks (1) (pentagonal grain diameter $d \approx 7$ mm, drum diameter $\approx 85\ d$). The drum rests on a wheel (2) driven by a stepper motor. The driving wheel rests on an electromagnetic shaker (3). The drum rests on freely rotating wheels (4) and is supported vertically by brackets. The dashed box shows the approximate region of grains imaged on the right.

with a flexible coupling and rests on an electromagnetic shaker to allow vertical vibration during rotation of the drum. Velcro is attached to both the driving wheel and the circumference of the rotating drum to maintain continuous contact between the drum and the driving wheel during vibration. We attach an accelerometer to the drum before and after each run to measure the vertical acceleration of the drum due to the imposed vibration. We characterize the imposed vibration by using the dimensionless acceleration [18,40] (peak acceleration relative to gravitational acceleration) $\Gamma = A(2\pi f)^2/g$. In this study, vibration is imposed at a frequency $f = 30$ Hz with a variable amplitude $A = 0$–$0.6$ mm, such that $\Gamma = 0$–$2$.

The drum is illuminated from behind and observed from the front. A digital camera is used to image the particles over time (typically at 5 Hz), and sequences of approximately 100 000 images per run are analyzed. This typically captures a few thousand avalanches per run. The primary measurement is the average angle of the interface versus time $\theta(t)$, which is computed automatically for each image by thresholding and edge detection algorithms. The extracted outline of the surface in the imaging region is fit to a straight line, and the average angle of the slope relative to horizontal is measured, such that an angle of $\theta = 0^\circ$ corresponds to a horizontal surface. From this, we determine the critical angle $\theta_c$ at which each failure occurs and the angle of repose $\theta_r$ which is reached after failure, and related properties such as interfacial roughness, mass transport, and mixing parameters. In this paper we focus on measurements of the surface angle $\theta(t)$.

Figure 2 shows a typical time series in which the angle steadily increases, as the granular material rotates as a rigid body, until a sudden failure of the surface occurs. The analysis described above defines an alternating sequence of critical and repose angles ($\theta_c$ and $\theta_r$). We refer to the gradual increase and rapid decrease of the surface angles as build-up and avalanche events with magnitudes $\Delta\theta = \theta_c - \theta_r$. Note that angles of repose for pentagons in two dimensions are larger than observed in three-dimensional materials, including spheres, as may be expected for faceted shapes deviating from spherical (or circular in two dimensions) symmetry [33].

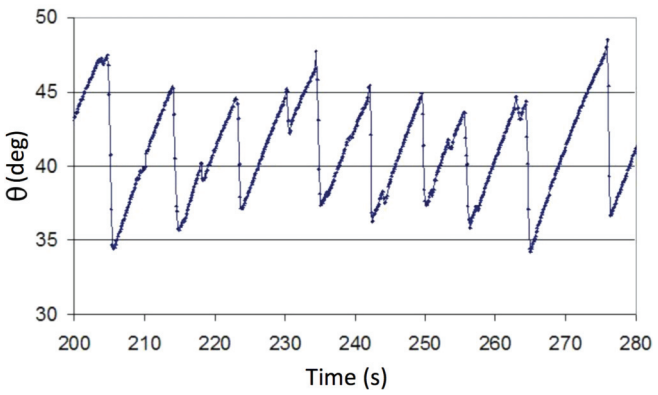


FIG. 2. (Color online) Typical measurement of average angle of the granular surface relative to horizontal versus time $\theta(t)$. The slope of the interface steadily increases during build-up as the drum rotates until a sudden failure corresponding to an avalanche. Angles in this and all subsequent figures are measured in degrees.

## III. AVALANCHE STATISTICS WITHOUT IMPOSED VIBRATION

Individual avalanche events are highly variable. We show statistics below, typically including multiple runs of over 100 000 images corresponding to a few thousand avalanches. In each run, the drum is rotated for at least two revolutions before collecting data to exclude initial transients. In the plot of interface slope versus time (Fig. 2), the angle increases at a constant rate due to the constant rotation of the drum until an avalanche occurs. Time series of the angle are analyzed to determine the start and end of the build-up and avalanche events. The start of an avalanche $\theta_c$ is determined when an increasing slope first begins to decrease and the end of the avalanche $\theta_r$ is the minimum angle reached before the angle again begins to increase. A threshold can also be included to set a minimum feature size counted as an avalanche, but the statistics presented here are found to be independent of threshold for thresholds up to $1^\circ$. Since this is an average slope across the surface, a few grains must move in order to register an avalanche.

In Fig. 3 we show the distributions, with Gaussian fits, for the angles of failure (mean critical angle: $\langle\theta_c\rangle = 44.5 \pm 0.05^\circ$, standard deviation: $\sigma = 3.2^\circ$) and the angle of repose ($\langle\theta_r\rangle = 39.3 \pm 0.06^\circ, \sigma = 3.4^\circ$) reached after failure for an individual run. The uncertainties are determined assuming simple statistical variation for $N \approx 3500$ independent avalanches, e.g., $\sigma/\sqrt{N} = 0.05^\circ$. The distributions are of comparable width, with significant overlap, in contrast to distributions observed for monodispersed glass beads [8]. During a particular event, the magnitude of the avalanche event, as measured by the change in angle $\Delta\theta = \theta_c - \theta_r$ is distributed as shown in Fig. 4. In this plot we show distributions of both the build-up (gradual increase from minimum to maximum angle) and avalanche (rapid failure of a large angle slope to a smaller angle) on a log-log scale. While the range of data is limited due to the system size, we observe a prevalence of small events and an approximately power-law distribution of large events ($\Delta\theta > 10^\circ$).

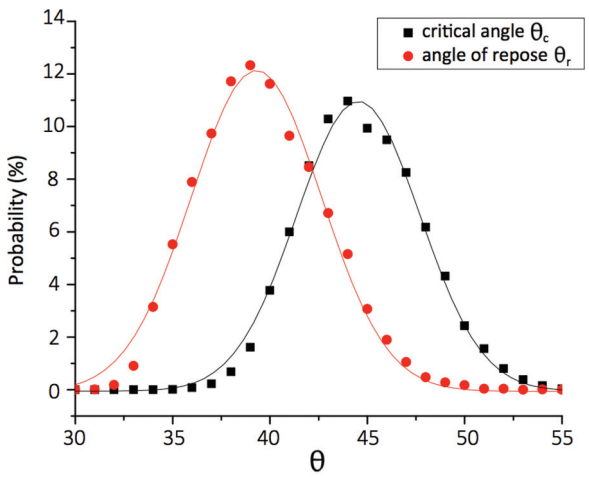


FIG. 3. (Color online) Probability distribution for the critical angle $\theta_c$ at which failure occurs and resulting angle of repose $\theta_r$ after an avalanche.

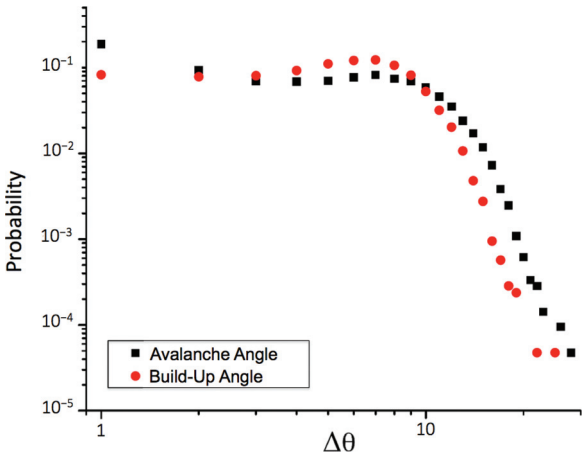


FIG. 4. (Color online) Probability distribution of avalanche size ($\Delta\theta = \theta_c - \theta_r$). Distributions for the magnitudes of both build-up (gradual increase in surface angle preceding an avalanche) and avalanche events (rapid decrease in surface angle) are shown.

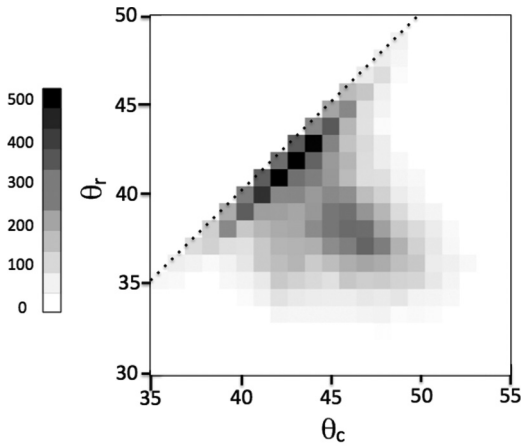


FIG. 6. Distribution of the angle of repose $\theta_r$ reached after an avalanche at a given critical angle $\theta_c$. Darker regions indicate a larger number of events. By definition, $\theta_r < \theta_c$; therefore events are distributed below the the dotted line, which indicates $\theta_r = \theta_c$.

As seen in the distributions plotted in Fig. 5, avalanches are correlated with the previous build-up events (Fig. 5, left) and anticorrelated with the size of the previous avalanche (Fig. 5, right). Darker regions indicate higher probability, and a nonlinear scale is used to highlight the qualitative features of the distribution. Large avalanches are likely to occur after long build-up events. Large events also typically follow small avalanches, though since small avalanches are more prevalent, it is expected that large avalanches will generally precede and follow smaller avalanches.

In Fig. 6 we show for a particular run a probability distribution of avalanche events in which a failure at a particular critical angle $\theta_c$ produces a resulting angle of repose $\theta_r$. By definition, $\theta_r < \theta_c$, so all events appear below the dotted line which indicates $\theta_r = \theta_c$. It is apparent that there are many small avalanches forming a line of high probability with $\theta_r \lesssim \theta_c$. In addition, there is a broad peak of avalanches which start at a critical angle of 44–47° resulting in an angle of repose of 36–40°, which reflects the peaks of the distributions observed in Fig. 3.

Photoelastic grains are used, which allow measurements of forces exerted on the grains [42]. When placed between crossed polarizers, compressive forces are imaged as photoelastic fringes, with grains under stress appearing bright and unstressed grains dark. While extremely sensitive, the photoelastic effect on a particular grain is proportional to the compressive force, in this case due to the weight of the grains above it. Therefore, measurements in the surface layers where flow occurs is difficult due to the small forces involved. Difference images, in which subsequent images are subtracted to highlight changes between images, are more sensitive to force changes, but also show locations where grain motion has occurred. Figure 7 shows a difference image in a 0.4 s interval during a single avalanche, in which grain motions can be seen with filamentary force chains appearing (black) and disappearing (white) below. We note though that observable

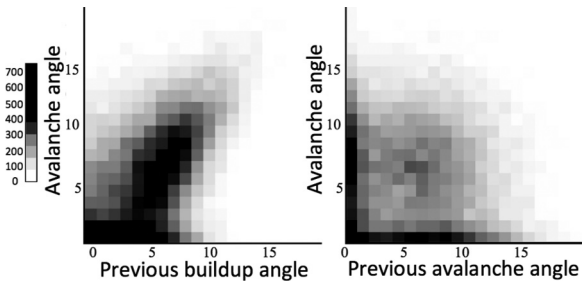


FIG. 5. Distribution of avalanche size versus size of previous build-up (left) and avalanche size versus previous avalanche (right). All angles are build-up and avalanche magnitudes $\Delta\theta$ as described in the text. Darker regions correspond to larger number of events. The scale is nonlinear to emphasize the shape of the distribution. Avalanches are correlated with the size of the previous build-up and anticorrelated with the size of the previous avalanche.

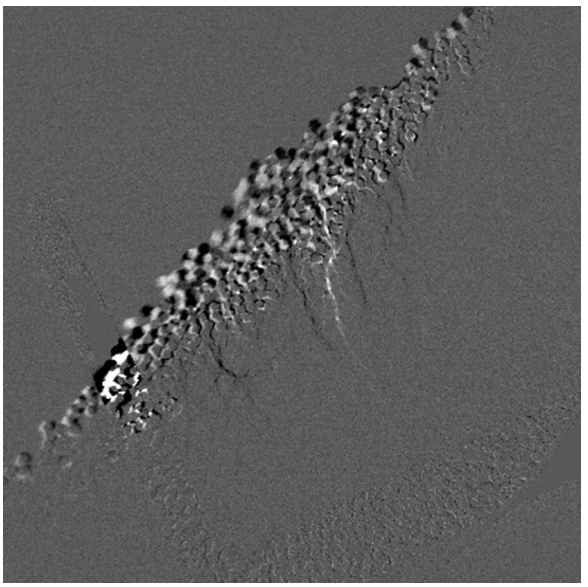

FIG. 7. Difference of photoelastic images during avalanche. Gray pixels indicate regions for which there has been no change in this time interval. Both grain motions and filamentary changes in force chains are visible in the surface layer as white (new) and black (old) pixels, with little change observed below the first 8–10 surface layers.

changes in both particle positions and forces are localized at the surface with essentially no change observed below the first 8–10 grain diameters, comparable to the depth of the flowing layer observed in similar experiments on glass beads [12].

## IV. AVALANCHE STATISTICS WITH VERTICAL VIBRATION

We now turn our attention to the effects of externally imposed vertical vibration on avalanche statistics in the rotating drum. Statistics presented in Sec. III can now be repeated with external vibration imposed. In Fig. 8 we show the mean critical angle $\langle\theta_c\rangle$ versus the dimensionless vibration acceleration, which shows the average critical (failure) angle determined from time series of the slope of the interface as in the previous section. At $\Gamma = 0$, the critical angle is considerably lower than the trend for larger dimensionless accelerations $\Gamma \geqslant 0.2$. We note that each data point represents an average of multiple individual runs and thousands of avalanches. As observed in Fig. 3, a typical standard deviation of $\sigma \approx 3^\circ$ with $N \approx 3500$ independent avalanches results in an uncertainty of the mean of $\sigma/\sqrt{N} \approx 0.05^\circ$, which appears unreasonably small compared to the fluctuations between data points. This suggests that avalanches in a given run are not statistically independent and that some effects of history dependence remain which are evidenced in run-to-run variability. To reflect this variation, the error bars indicate the variance in the mean critical values for the individual runs. That is, we take the standard deviation of the mean critical angles $\langle\theta_c\rangle$ for each data point in Fig. 8, which typically includes 3−4 independent runs, and use the average value ($\sigma = 0.8$) to indicate the variance in the values plotted. As we collected significantly more data for $\Gamma = 0$ (corresponding to 22 000 avalanches), we compute the standard deviation of the mean for these data sets separately ($\sigma = 0.45$) The variance based on the scatter between runs at the same acceleration is consistent with the observed scatter in the mean values plotted in Fig. 8.

We plot probability distributions for $\theta_c$ and corresponding Gaussian fits for one individual run at $\Gamma = 0$, 0.2, and 0.4

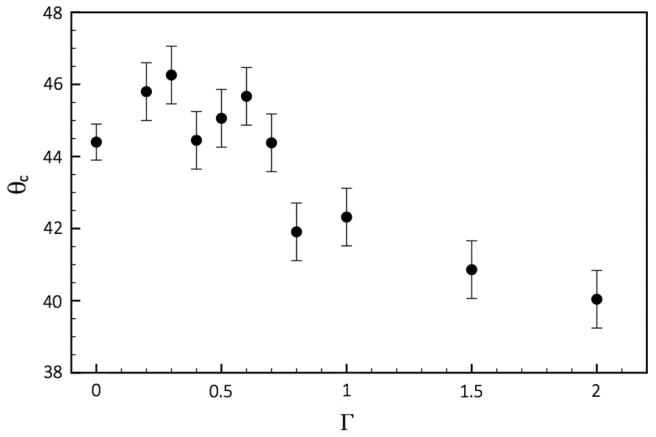


FIG. 8. Critical angle $\theta_c$ versus dimensionless external vibration acceleration $\Gamma$ showing a peak critical angle at nonzero imposed vibration ($\Gamma \approx 0.3$). Error bars represent the variance of mean critical angles for individual runs as described in the text. With increasing vibration for $\Gamma < 0.2$, an increase in critical angle is observed.

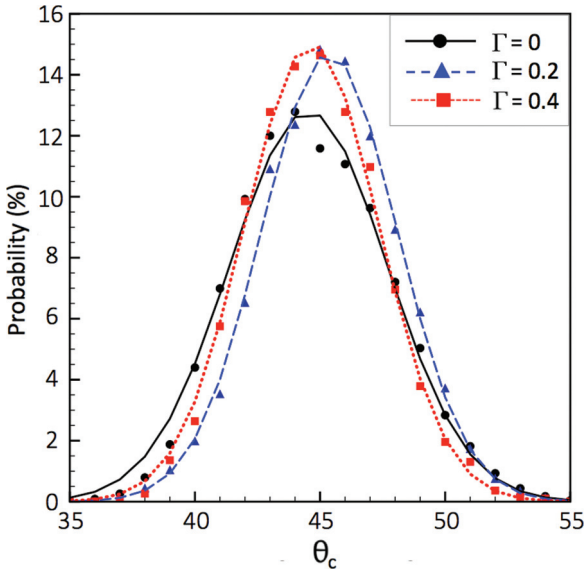


FIG. 9. (Color online) Probability distributions of critical angles $\theta_c$ for three individual runs with dimensionless acceleration $\Gamma = 0$, 0.2, and 0.4. The solid lines show Gaussian fits with corresponding mean critical angles $\langle\theta_c\rangle = 44.5^\circ$, $45.4^\circ$, and $44.6^\circ$ ($\pm 0.1^\circ$) and standard deviations $\sigma = 3.1^\circ$, $2.7^\circ$, and $2.7^\circ$, respectively.

in Fig. 9, which shows the variations between runs. As we expect, the typical variation of the mean values of 1–2° is small compared to the widths of the distributions, $2\sigma \approx 7^\circ$, but larger than the uncertainties in the mean values ($\sigma/\sqrt{N} = 0.1^\circ$). We find over multiple runs for each data point that the average critical angle at zero acceleration is below what might be projected based on the trend in the data for $\Gamma \geqslant 0.2$, with a subsequent decrease in mean critical angle for larger vibrations. We also note that the mean critical value at $\Gamma = 0$ is lower than each of the seven individual runs which comprise the data points at $\Gamma = 0.2$ and 0.3.

The increase in critical angle for small vibrations may be expected based on the fact that granular systems typically compact with small amplitude vibrations [15] and that shear modulus increases dramatically with packing fraction for granular samples. A small vibration likely leads to compaction and relaxation of frictional contacts, both of which would lead to an increase in the stability of the slope, while a large vibration provides sufficient energy to destabilize the slope. Ongoing work using this experimental setup [43] indicates that in a loosely packed static pile, vibration leads to an initial increase in density of up to 5% within 10–20 s, followed by an additional relaxation of up to 1% in a time frame of minutes, consistent with earlier measurements of compaction for small vibration accelerations [15]. While we observe rigid rotation of the bulk region, vibration-induced compaction likely occurs in the surface layer after an avalanche, providing a mechanism for the observed strengthening for small $\Gamma$.

We note that a relatively steep angle is still maintained even for $\Gamma > 1$ since the small vibration amplitude ($\geqslant 0.04\,d$) does not lead to significant rearrangement of the interlocked pentagonal grains. In this case a simple Coulomb block model [26], which would predict instability at $\Gamma = 1$, does not apply. We also note that qualitatively at higher accelerations

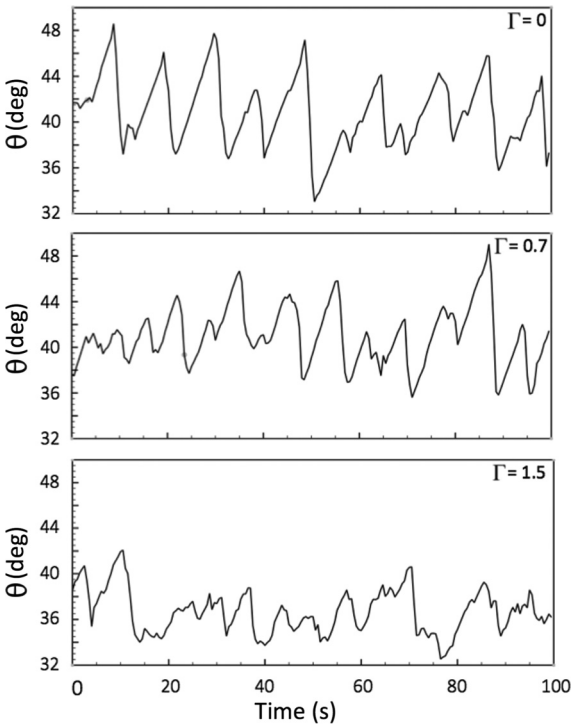


FIG. 10. Interface angle versus time $\theta(t)$ with changes in external vibration ($\Gamma = 0, 0.7, 1.5$).

$\Gamma > 2$ the average angle continues to drop. At larger vibration amplitudes, the interface also exhibits a more continuous "slumping" behavior as is seen at higher velocities without vibration [44]. In Fig. 10 we show the angle of the interface versus time with changes in vibration acceleration.

To isolate the effects of the vibration from rotation, we show the behavior of the system when a stationary, inclined surface is subjected to vibration in Fig. 11. In this case the pile is rotated to a large angle, close to, but below, the critical angle in the absence of vibration. The drum is stopped, and vibration is then started. Here we show difference images, in which images before and after the avalanche are subtracted from each other to show changes during the avalanche. Regions where no change has occurred between frames appear as gray while grains are observed to move from regions with black pixels to regions with white pixels. For the two vibration amplitudes shown, the effects appear to be limited to the surface, without observable changes in the bulk, though the mass of material displaced and the depth of the disturbance increases with vibration amplitude. This is consistent with prior results on nonvibrated rotating drums (see, for example, Ref. [10]). The present results suggest that vibrations of $\Gamma < 2$ lead to destabilization of the surface grains that are near failure rather than disrupting the bulk contact network. Additionally, while granular samples often contain "rattler" grains not constrained by their neighbors, which are able to move within the cage formed by surrounding neighbors, their absence here is consistent with recent observations that rattlers are infrequently observed in 2D packings of angular or nonspherical particles [45]. Further results on compaction dynamics will be presented elsewhere [43].

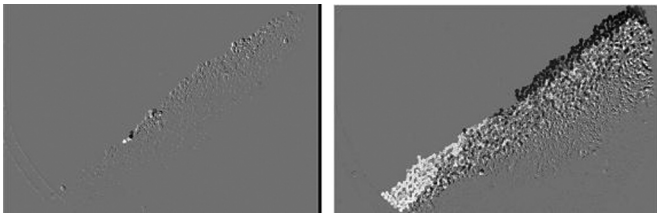

FIG. 11. Difference images showing motion of grains for a stationary (nonrotating), high angle slope subjected to small ($\Gamma = 0.4$) and large ($\Gamma = 2$) vibrations. An image before vibration is subtracted from an image after steady state is reached.

## V. HISTORY DEPENDENCE IN AN OSCILLATED SYSTEM

In order to ascertain the importance of preexisting textures in the granular material, we characterize the avalanching behavior after reversing the shearing direction. We oscillate the drum, observing approximately 50 rotations in one direction before reversing the direction of rotation. In Fig. 12 we show a small portion of a time series in which many avalanches occur as the drum rotates clockwise, similar to Fig. 2, before the drum is reversed, rotating in the opposite directions (for which the angle is negative) and leading to a series of avalanches as the drum rotates counterclockwise. We group the critical angles for the initial avalanches (immediately after the rotation direction was changed) as well as the subsequent avalanches, which represent the steady-state critical angle distribution reached during continuous rotation. History dependence is evident as the deviation between the distribution of the critical angles for the initial failure compared to the steady-state distribution. We then repeat this sequence for a variety of vibration amplitudes. Runs of a few thousand avalanches are necessary as we measure one initial avalanche data point for approximately every 50 steady-state avalanches.

Histograms of these critical angles are shown in Fig. 13 for imposed vibrations of $\Gamma = 0, 0.4$, and 0.8 along with Gaussian fits. There, it is evident that at zero imposed vibration, the distribution of the initial critical angle is shifted to the left compared to the steady-state distribution. That is, the initial critical angle is smaller than at steady state, and the pile is less stable upon reversal, suggesting that the texture within the pile evolves to produce a pile that withstands continued shear in the same direction more effectively than shear in the reverse direction. This is consistent with similar measurements made

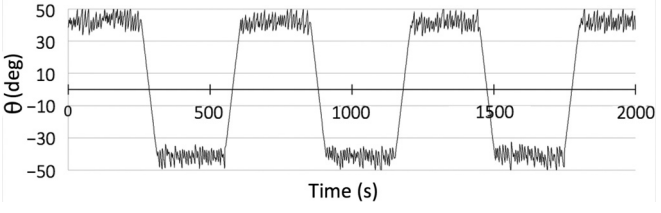


FIG. 12. Time series for oscillated rotating drum $\theta(t)$. Many avalanches are observed, and steady state is achieved before reversing the direction of rotation.

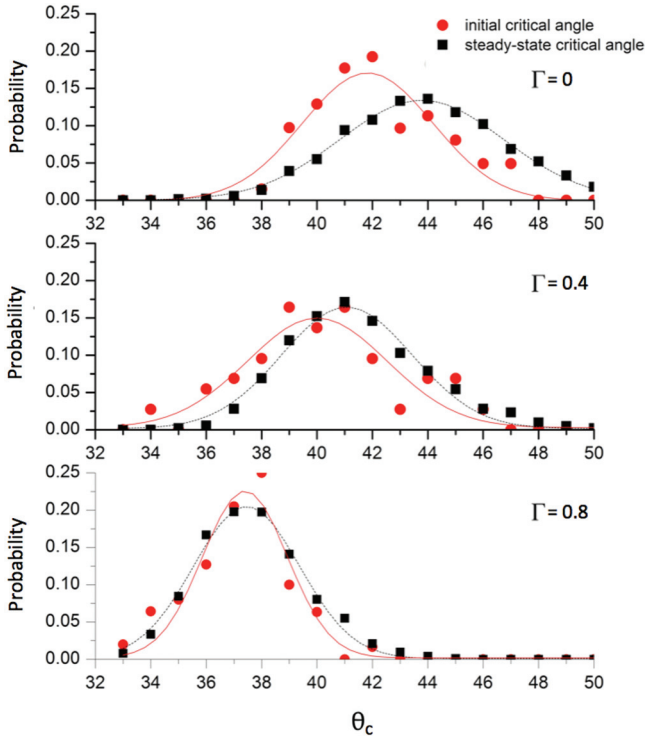


FIG. 13. (Color online) Histogram of critical angles $\theta_c$ upon reversal of drum rotation at imposed vibrations of $\Gamma = 0$, 0.4, and 0.8. Critical angles for the initial avalanche upon reversal are binned separately from the steady-state critical angle distribution for avalanches during continuous rotation. History dependence is observed as a relative shift of initial avalanches compared to steady state, which is removed for external vibrations of $\Gamma \geqslant 0.8$.

on transients in a Couette shear apparatus upon reversal of shear direction [34,37].

As the vibration amplitude is increased, both initial and steady-state critical angles decrease as the vibration induces failure. In addition, with increasing vibration, the separation between the peaks of the distributions for the initial avalanche versus steady state decreases. To lowest order, this separation decreases monotonically with vibration acceleration, but given that the sample size of first avalanches is 50 times smaller than subsequent avalanches, we are not able to resolve an explicit relationship. Beyond shaking accelerations of $\Gamma = 0.8$, the distributions overlap within measurement uncertainty. That is, at large vibration amplitudes the effective memory, or history dependence, of the pile is erased. We emphasize that the pile still maintains a substantial angle of repose ($\theta \approx 38^\circ$) for the strongly interlocking pentagonal grains used (well above that for vibrated glass spheres), but the vibration induces substantial agitation and settling of the surface layers which dictate avalanching behavior.

## VI. DISCUSSION

Experiments on granular avalanches in a rotating drum produce time series of the average surface angle which allows a variety of statistics to be measured. Primary results include the fact that under external vibration, a granular slope is stabilized with small vibrations ($\Gamma \leqslant 0.2$), due to compaction and relaxation of frictional contacts, and destabilized at larger imposed vibration. Therefore, while external vibration may broadly be thought of as a destabilizing factor, the degree of compaction is a critical variable which may lead to strengthening relative to the nonvibrated case. Though compaction is likely the dominant factor and the focus of ongoing work [43], relaxation of frictional contacts near failure may also contribute.

These experimental results specifically focus on pentagonal grains, whose flat sides lead to strong geometric constraints on flow. In addition to observing large surface angles compared to spherical grains [20,33], even with external vibration, we find that the critical angle and angle of repose display wide, overlapping distributions, unlike prior experiments using glass spheres [8]. Vibration amplitudes used are still small relative to the roughness of the pentagonal grains and vibration effects in smooth or spherical shapes may be more evident, with a faster onset as vibration amplitude is increased. Qualitative features though, such as a power-law distribution for large avalanches appear similar to prior results [41].

In addition, history dependence is observed when the rotation direction is changed, as the probability distribution for the critical angle of the initial failure is measurably different than the distribution observed for long runs at continuous rotation in one direction. Similar to experiments which show weakening under shear reversal [34,35,37], piles constructed through rotation develop a texture that makes the pile more resistant to continued shear in the same direction and more fragile with a reversal of shear direction. Imaging shows that vibration effects are confined to the surface layers and that the bulk material rotates as a rigid body, as in nonvibrated rotating drum experiments [10–12]. We propose that external vibration agitates the surface layer specifically, which comprise the grains leading to avalanches, and removes the history dependence by disrupting the static force network developed during shear and compacting the sample. The strong history dependence of granular systems makes avalanche prediction difficult, but continuously agitated systems may provide a reproducible steady state with flow properties that do not exhibit history dependence.

## ACKNOWLEDGMENTS

We gratefully acknowledge the support of the Research Corporation (Cottrell College Science Award No. CC7145/7266) and DOD ASSURE Grant No. DMR-0353773.

[1] Eur. Phys. J. E **14**, 341 (2004).
[2] Y. Forterre and O. Pouliquen, Annu. Rev. Fluid Mech. **40**, 1 (2008).
[3] C. Ancey, J. Non-Newtonian Fluid Mech. **142**, 4 (2007).
[4] J. M. Ottino and D. V. Khakhar, Annu. Rev. Fluid Mech. **32**, 55 (2000).
[5] A. J. Liu and S. Nagel, Nature (London) **396**, 21 (1998).
[6] J. Rajchenbach, Phys. Rev. Lett. **88**, 014301 (2001).

[7] A. Kabla, G. Debrgeas, J. Di Meglio, and T. J. Senden, Europhys. Lett. **71**, 932 (2005).
[8] R. Fischer, P. Gondret, B. Perrin, and M. Rabaud, Phys. Rev. E **78**, 021302 (2008).
[9] R. Fischer, P. Gondret, and M. Rabaud, Phys. Rev. Lett. **103**, 128002 (2009).
[10] J. M. N. T. Gray, J. Fluid Mech. **441**, 1 (2001).
[11] A. V. Orpe and D. V. Khakhar, Phys. Rev. E **64**, 031302 (2001).
[12] G. Félix, V. Falk, and U. D'Ortona, Eur. Phys. J. E **22**, 25 (2007).
[13] I. C. Christov, J. M. Ottino, and R. M. Lueptow, Phys. Rev. E **81**, 046307 (2010).
[14] K. M. Hill and J. Kakalios, Phys. Rev. E **52**, 4393 (1995).
[15] E. Nowak *et al.*, Powder Technol. **94**, 79 (1997).
[16] P. Richard, P. Philippe, F. Barbe, S. Bourles, X. Thibault, and D. Bideau, Phys. Rev. E **68**, 020301 (2003).
[17] F. Melo, P. Umbanhowar, and H. L. Swinney, Phys. Rev. Lett. **72**, 172 (1994).
[18] P. B. Umbanhowar, F. Melo, and H. L. Swinney, Nature (London) **382**, 793 (1996).
[19] G. A. Caballero-Robledo and E. Clément, Eur. Phys. J. E **30**, 395 (2009).
[20] H. M. Jaeger, C. H. Liu, and S. R. Nagel, Phys. Rev. Lett. **62**, 40 (1989).
[21] G. Metcalfe, S. G. K. Tennakoon, L. Kondic, D. G. Schaeffer, and R. P. Behringer, Phys. Rev. E **65**, 031302 (2002).
[22] C. R. Wassgren *et al.*, Phys. Fluids **14**, 3439 (2002).
[23] P. Sistla, O. Baran, Q. Chen, S. Fohanno, P. H. Poole, and R. J. Martinuzzi, Phys. Rev. E **71**, 011303 (2005).
[24] K. Kim, J. K. Moon, J. J. Park, H. K. Kim, and H. K. Pak, Phys. Rev. E **72**, 011302 (2005).
[25] D. Rubin, N. Goldenson, and G. A. Voth, Phys. Rev. E **74**, 051307 (2006).
[26] P. J. King, M. R. Swift, K. A. Benedict, and A. Routledge, Phys. Rev. E **62**, 6982 (2000).
[27] L. Staron, J.-P. Vilotte, and F. Radjai, Phys. Rev. Lett. **89**, 204302 (2002).
[28] L. Staron, F. Radjai, and J.-P. Vilotte, J. Stat. Mech.: Theory Exp. (2006) P07014.
[29] S. J. Linz and P. Hänggi, Phys. Rev. E **50**, 3464 (1994).
[30] J. M. Luck and A. Mehta, J. Stat. Mech. (2004) P10015.
[31] M. Ciamarra, A. Coniglio, and M. De Martino, and D. Nicodemi, Eur. Phys. J. E **24**, 411 (2007).
[32] A. M. Vidales, L. A. Pugnaloni, and I. Ippolito, Granular Matter **11**, 53 (2009).
[33] G. S. Riley and G. R. Mann, Mater. Res. Bull. **7**, 163 (1972).
[34] B. Utter and R. Behringer, Eur. Phys. J. E **14**, 373 (2004).
[35] S. Deboeuf, O. Dauchot, L. Staron, A. Mangeney, and J.-P. Vilotte, Phys. Rev. E **72**, 051305 (2005).
[36] F. Radjai, D. E. Wolf, M. Jean, and J. J. Moreau, Phys. Rev. Lett. **80**, 61 (1998).
[37] M. Toiya, J. Stambaugh, and W. Losert, Phys. Rev. Lett. **93**, 088001 (2004).
[38] Y. Grasselli and H. J. Herrmann, Physica A **246**, 301 (1997).
[39] J. A. Dijksman, G. H. Wortel, L. T. H. van Dellen, O. Dauchot, and M. van Hecke, Phys. Rev. Lett. **107**, 108303 (2011).
[40] H. K. Pak and R. P. Behringer, Phys. Rev. Lett. **71**, 1832 (1993).
[41] S. Y. Lehman *et al.*, Granular Matter **14**, 553 (2012).
[42] B. Utter, in *Experimental and Computational Techniques in Soft Condensed Matter Physics*, edited by J. Olafsen (Cambridge University Press, Cambridge, 2010), pp. 230–247.
[43] N. Swisher and B. C. Utter (unpublished).
[44] J. M. Xiao, Yan Liu, and Eckehard Specht, Chem. Eng. Sci. **60**, 3629 (2005).
[45] Y. Jiao, F. H. Stillinger, and S. Torquato, Phys. Rev. E **81**, 041304 (2010).